



## IMPLEMENTATION OF DRBEM FOR THE DETERMINATION OF THE HEAT FLUX IN AN INVERSE PROBLEM

Nagehan ALSOY AKGÜN

Department of Mathematics, Van Yüzüncü Yıl University, Van, TURKEY

**ABSTRACT.** A numerical investigation of inverse unsteady natural convection flow in a square cavity filled with  $Cu$ -water nanofluid is performed. In the direct problem, the enclosure is bounded by one isothermally heated vertical wall at temperature  $T_m$  and by three adiabatic walls. In the inverse problem, the enclosure is bounded by right hostile wall on which no boundary condition can be prescribed or measured and by left accessible wall on which both the boundary temperature and heat flux data are overspecified. The dual reciprocity boundary element method (DRBEM) with the fundamental solutions of Laplace and modified Helmholtz equations is used for the solutions of direct and inverse problems. Inhomogeneities are approximated with radial basis functions. Computations are performed for several values of Rayleigh number ( $Ra$ ), solid volume fraction ( $\phi$ ) and percentage of noise ( $\rho$ ), and accurate and stable results are given for three forms of heat flux namely, steady heat flux ( $q = q(y)$ ), time dependent uniform heat flux ( $q = q(t)$ ) and non-uniform time dependent heat flux ( $q = q(y, t)$ ).

### 1. INTRODUCTION

In the thermo-fluid areas, flow heat transfer analysis is one of the most interesting subject among the researchers. The researchers who study in this area focused to the idea of using nanofluid instead of a using conventional heat transfer base fluids with the low thermal conductivity such as water, engine oil etc. Nanofluid is the combination of the base fluid and added nanoparticles, and this term is made use of for the first time by Choi in [1]. The aim of using nanofluids is to increase the thermal performance of conventional fluids. Some studies published as review on nanofluids can be found in [2]- [9].

---

2020 *Mathematics Subject Classification.* Primary 65N20, 65N21; Secondary 65N38, 35Q35.

*Keywords and phrases.* DRBEM, inverse problem, natural convection, nanofluid.

✉ nagehanalsoyakgun@yyu.edu.tr

ORCID 0000-0001-6967-0625.

In some applications of heat transfer, because of the high temperature it may not be possible to measure of boundary conditions on some part of the surface. The non-measurable temperature or heat flux boundary conditions can be determined by the temperature measurements from the other parts of the surface or inside of the body. The estimation of temperature or heat flux boundary conditions is called inverse heat conduction problem for temperature and the excellent study about this subject has been done by Beck et al. [10]. After that, a number of studies for the inverse problem have been published in [11]- [16]. An inverse forced-convection problem in a channel has been investigated in [11] while convection-diffusion equation has been solved in [12]- [14]. In addition, advection-diffusion and reaction-diffusion equations for an inverse problem case have been considered in [15] and [16], respectively. Later on, one-dimensional inverse heat conduction problem has solved in [17].

The inverse natural convection flow has been solved by using a solution algorithm based on the sequential function specification method in [18], and by using an implicit control volume discretization procedure in [19]. Also, DRBEM applications have been presented for the inverse natural convection flow under a magnetic field problem in [20] and for the Magneto hydrodynamics (MHD) flow problem in [21]. In all these studies mentioned above, the governing equations are coupled nonlinearly which leads to extra difficulty for the inverse problem.

The purpose of this study is to solve the inverse natural convection of copper based nanofluid problem using different type heat flux boundary conditions. To do this aim, computations are carried using for three types of adiabatic boundary conditions, namely, steady heat flux ( $q(y) = -\cos(\pi y)$ ), time dependent uniform heat flux ( $q(t) = -\sin(\pi t/t_f)$ ) and non-uniform time dependent heat flux ( $q(y, t) = -\sin(\pi t)\cos(\pi y)$ ). Since the analytical solution of corresponding direct problem is not available, it is necessary to solve the corresponding direct problem using any numerical method. In this study both direct and inverse problems are solved using DRBEM. In the DRBEM procedure, it is only necessary to discretize the boundary of the domain to be analyzed, so it requires less storage and less computing time.

The fundamental concepts about this method can be found in [22]. Since DRBEM uses the fundamental solution of differential equation for converting the domain integral into a boundary integral, the original differential equation should be written as a differential equation whose fundamental solution can be obtained. In this current work, vorticity transport and temperature equations are written in the forms of modified Helmholtz equations by considering all the nonlinear terms as the non-homogeneous terms.

A well-posed problem in generally can be defined as a mathematical problem where its solution(s) has/have three properties namely existence, uniqueness and stability. If any of these three properties mentioned above fail then the problem becomes an ill-posed problem and this kind of a problem is called an inverse problem. Due to the ill-posedness property of the problem, the small errors occurred in the measurement causes the big deviations in the inverse solution. Therefore,

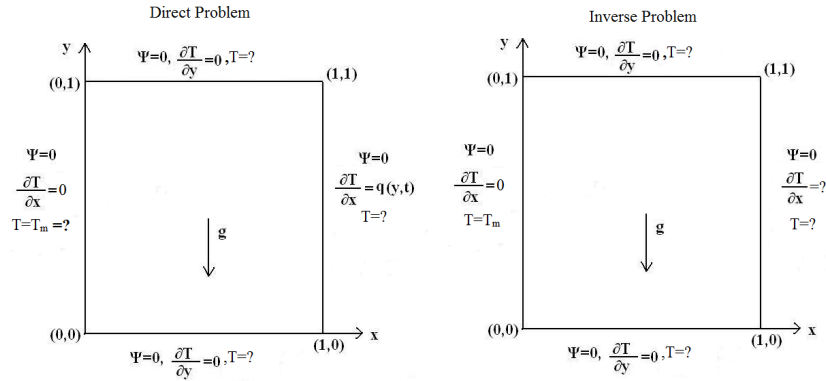


FIGURE 1. Schematic diagram of the domain.

Tikhonov regularization method [23] have been utilized to regularize ill-posedness of the problem.

The inverse natural convection in a nanofluid filled cavity presented in this study has not been considered and investigated yet. This article is planned in the following way. In Section 2 definition of the direct and inverse problems are given. Section 3 contains the mathematical model of the governing equations. DRBEM is described for both direct and inverse problems in Section 4. Results based on numerical simulation are discussed and presented for three types of heat flux boundary conditions in Section 5. Finally, Section 6 presents the conclusions obtained from this study.

## 2. DEFINITION OF THE DIRECT AND INVERSE PROBLEMS

Consider the two-dimensional unsteady equations of motion and energy for nanofluid (*Cu*-water) in the non-dimensional velocity ( $u, v$ ), pressure ( $p$ ) and temperature ( $T$ ) form as

$$\frac{\partial u}{\partial x} + \frac{\partial v}{\partial y} = 0, \tag{1}$$

$$\frac{\partial u}{\partial t} + u \frac{\partial u}{\partial x} + v \frac{\partial u}{\partial y} = -\frac{\partial p}{\partial x} + \frac{\mu_{nf}}{\rho_{nf} \alpha_f} \nabla^2 u, \tag{2}$$

$$\frac{\partial v}{\partial t} + u \frac{\partial v}{\partial x} + v \frac{\partial v}{\partial y} = -\frac{\partial p}{\partial y} + \frac{\mu_{nf}}{\rho_{nf} \alpha_f} \nabla^2 v + RaPr \frac{(\rho\beta)_{nf}}{\rho_{nf} \beta_f} T, \tag{3}$$

$$\frac{\partial T}{\partial t} + u \frac{\partial T}{\partial x} + v \frac{\partial T}{\partial y} = \frac{\alpha_{nf}}{\alpha_f} \nabla^2 T, \tag{4}$$

where  $\mu$ ,  $\rho$ ,  $\alpha$ , and  $\beta$  are dynamic viscosity, effective density, thermal diffusivity and thermal expansion coefficient, respectively. The above non-dimensional equations are obtained by using the following non-dimensional variables

$$\begin{aligned} x &= \frac{x'}{L_0}, & y &= \frac{y'}{L_0}, & u &= \frac{u' L_0}{\alpha_f}, & v &= \frac{v' L_0}{\alpha_f}, & T &= \frac{T' - T_c}{\Delta T}, \\ p &= \frac{p' L_0^2}{\rho_{nf} \alpha_f^2}, & t &= \frac{t' \alpha_f}{L_0^2}, & Ra &= \frac{g \beta_f L_0^3 \Delta T}{\nu_f \alpha_f}, & Pr &= \frac{\nu_f}{\alpha_f}, \end{aligned} \quad (5)$$

where  $L_0$ ,  $g$ ,  $\nu$  and  $\Delta T = T_{hot} - T_{cold}$  are the characteristic length, gravitational acceleration, kinematic viscosity and temperature difference, respectively. Also,  $Ra$  is the Rayleigh number and  $Pr$  is the Prandtl number. The prime in Equation (5) refers that the variables are dimensional.

The thermo-physical properties of the nanofluid, water and copper can be given as in [24] by

$$\begin{aligned} \rho_{nf} &= (1 - \phi)\rho_f + \phi\rho_s, & \alpha_{nf} &= \frac{k_{nf}}{(\rho C_p)_{nf}}, \\ (\rho C_p)_{nf} &= (1 - \phi)(\rho C_p)_f + \phi(\rho C_p)_s, & \mu_{nf} &= \frac{\mu_f}{(1 - \phi)^{2.5}}, \\ (\rho\beta)_{nf} &= (1 - \phi)(\rho\beta)_f + \phi(\rho\beta)_s, & k_{nf} &= k_f \left( \frac{k_s + 2k_f - 2\phi(k_f - k_s)}{k_s + 2k_f + \phi(k_f - k_s)} \right), \end{aligned} \quad (6)$$

where  $\phi$  is nanoparticle volume fraction,  $k$  is thermal conductivity,  $(\rho C_p)_{nf}$  is heat capacitance,  $(\rho\beta)_{nf}$  is thermal expansion coefficient,  $\mu$  is dynamic viscosity and the subscripts ' $nf$ ', ' $f$ ' and ' $s$ ' refer to nanofluid, fluid and solid, respectively.

Two-dimensional unsteady equations of motion and energy for nanofluid in the non-dimensional stream function ( $\psi$ ), vorticity ( $w$ ) and temperature ( $T$ ) form can be defined as

$$\nabla^2 \psi = -w, \quad (7)$$

$$\frac{\mu_{nf}}{\rho_{nf} \alpha_f} \nabla^2 w = \frac{\partial w}{\partial t} + u \frac{\partial w}{\partial x} + v \frac{\partial w}{\partial y} - Ra Pr \frac{(\rho\beta)_{nf}}{\rho_{nf} \beta_f} \frac{\partial T}{\partial x}, \quad (8)$$

$$\frac{\alpha_{nf}}{\alpha_f} \nabla^2 T = \frac{\partial T}{\partial t} + u \frac{\partial T}{\partial x} + v \frac{\partial T}{\partial y}, \quad (9)$$

where

$$u = \frac{\partial \psi}{\partial y}, \quad v = -\frac{\partial \psi}{\partial x}, \quad w = \frac{\partial v}{\partial x} - \frac{\partial u}{\partial y}. \quad (10)$$

**2.1. Direct Problem:** The schematic of the physical situations of both direct and inverse problems, which have the same boundary conditions as those previously investigated in [19], are shown in Figure (1). The boundary conditions for the direct problem are

$$\psi(0, y, t) = \psi(1, y, t) = \psi(x, 0, t) = \psi(x, 1, t) = 0, \tag{11}$$

$$\frac{\partial T}{\partial x}(1, y, t) = q(y, t), \quad \frac{\partial T}{\partial x}(0, y, t) = \frac{\partial T}{\partial y}(x, 0, t) = \frac{\partial T}{\partial y}(x, 1, t) = 0. \tag{12}$$

where  $q(y,t)$  is the most general form of nondimensional heat flux boundary condition at  $x = 1$ . Vorticity boundary conditions are obtained using the Equation (10). Direct problem is subject to the initial conditions

$$w(x, y, 0) = T(x, y, 0) = 0. \tag{13}$$

**2.2. Inverse Problem:** In the inverse problem one of the terms (boundary conditions at the right wall) is not known explicitly for the temperature and it should be specified from a direct problem. In this study, the time varying temperature measurement ( $T_m$ ) at the left wall, which is given in Figure (1) and will be obtained by solving the direct problem, is considered as an overspecification for the compensation of the missing boundary condition at the right wall. Thus the temperature boundary conditions for the inverse problem are

$$T(0, y, t) = T_m, \quad \frac{\partial T}{\partial x}(0, y, t) = \frac{\partial T}{\partial y}(x, 0, t) = \frac{\partial T}{\partial y}(x, 1, t) = 0. \tag{14}$$

Stream function and vorticity boundary conditions are the same as the direct problem. Initial conditions for vorticity transport and temperature equations are also the same as the direct problem.

In the inverse problem, the small measurement errors appeared in the computation of the  $T_m$  can be caused the large errors. Thus, ill-posedness occurs in the inverse solution procedure. This means that the solutions  $T(1, y, t)$  and  $\frac{\partial T}{\partial x}(1, y, t)$  can be unstable. Therefore, in order to obtain a stable numerical solution for the inverse problem, regularization methods, for instance Tikhonovs regularization should be used in the solution procedure.

### 3. MATHEMATICAL MODEL

For the solution of both direct and inverse problems DRBEM will be used as a numerical technique and so we need to use fundamental solutions of the Laplace and modified Helmholtz equations. Stream function equation is in the form of Poisson equation and vorticity transport and energy equations are transformed to the nonhomogeneous modified Helmholtz equations. To do this aim first the time derivatives in the vorticity transport and energy equations are approximated by using the forward finite difference approximations

$$\frac{\partial w}{\partial t} = \frac{w^{(s+1)} - w^{(s)}}{\Delta t}, \quad \frac{\partial T}{\partial t} = \frac{T^{(s+1)} - T^{(s)}}{\Delta t}, \tag{15}$$

where  $w^{(s)} = w(x, y, t_s)$ ,  $T^{(s)} = T(x, y, t_s)$ ,  $t_s = s\Delta t$  and  $\Delta t$  is the time step. Then vorticity and temperature variables in the Laplace terms are also approximated at the two time levels by using relaxation parameters  $\theta_w$  and  $\theta_T$  as

$$\begin{aligned} w^{(s+1)} &= \theta_w w^{(s+1)} + (1 - \theta_w)w^{(s)}, \\ T^{(s+1)} &= \theta_T T^{(s+1)} + (1 - \theta_T)T^{(s)}. \end{aligned} \quad (16)$$

Inserting the approximations in Equations (15) and (16) into the related Equations (8) and (9), two nonhomogeneous modified Helmholtz equations are obtained for vorticity transport and energy equations

$$\nabla^2 \psi^{(s+1)} = -w^{(s)}, \quad (17)$$

$$\begin{aligned} \nabla^2 w^{(s+1)} - \lambda_w^2 w^{(s+1)} &= \frac{(\theta_w - 1)}{\theta_w} \nabla^2 w^{(s)} - \lambda_w^2 w^{(s)} \\ &+ \frac{\rho_{nf} \alpha_f}{\mu_{nf} \theta_w} \left( \frac{\partial \psi^{(s+1)}}{\partial y} \frac{\partial w^{(s)}}{\partial x} - \frac{\partial \psi^{(s+1)}}{\partial x} \frac{\partial w^{(s)}}{\partial y} \right) \\ &- RaPr \frac{(\rho\beta)_{nf} \alpha_f}{\beta_f \mu_{nf} \theta_w} \frac{\partial T^{(s)}}{\partial x}, \end{aligned} \quad (18)$$

$$\begin{aligned} \nabla^2 T^{(s+1)} - \lambda_T^2 T^{(s+1)} &= \frac{(\theta_T - 1)}{\theta_T} \nabla^2 T^{(s)} - \lambda_T^2 T^{(s)} \\ &+ \frac{\alpha_f}{\alpha_{nf} \theta_T} \left( \frac{\partial \psi^{(s+1)}}{\partial y} \frac{\partial T^{(s)}}{\partial x} - \frac{\partial \psi^{(s+1)}}{\partial x} \frac{\partial T^{(s)}}{\partial y} \right), \end{aligned} \quad (19)$$

where

$$\lambda_w^2 = \frac{\rho_{nf} \alpha_f}{\mu_{nf} \Delta t \theta_w}, \quad \lambda_T^2 = \frac{\alpha_f}{\alpha_{nf} \Delta t \theta_T}.$$

#### 4. DRBEM FORMULATION OF THE PROBLEM

The governing equations given in (17)-(19) for the direct and inverse formulations are solved by using DRBEM. DRBEM implementation of Poisson and modified Helmholtz equations for the inverse problem can be done by using the same way as the direct problem. The DRBEM discretization of the inverse problem leads to an ill-conditioned linear system of equations for temperature due to overspecified boundary conditions on the left wall and underspecified conditions on the right wall. In order to obtain the stable results, the ill-conditioned linear system of equations for temperature is regularized with Tikhonov regularization method. The governing equations in the form of Poisson and modified Helmholtz equations can be written in the compact forms as

$$\nabla^2 \psi^{(s+1)} = b_1, \quad (20)$$

$$\nabla^2 w^{(s+1)} - \lambda_w^2 w^{(s+1)} = b_2, \quad (21)$$

$$\nabla^2 T^{(s+1)} - \lambda_T^2 T^{(s+1)} = b_3, \tag{22}$$

where  $b_1, b_2, b_3$  are the right hand sides of corresponding equations (17)-(19). These right hand side functions contain the values of vorticity and temperature obtained from the previous time level and the values of stream function obtained from the current time level.

Equation (20) is weighted in domain by the fundamental solution  $u_\psi^* = \frac{1}{2\pi} \ln(r)$  of Laplace equation, and Equations (21) and (22) are weighted in domain by the fundamental solutions  $u_w^* = \frac{1}{2\pi} K_0(\lambda_w r)$  and  $u_T^* = \frac{1}{2\pi} K_0(\lambda_T r)$  of modified Helmholtz equations as in [25]. By applying the Green's second identity to the resulting weighted residual statements, left hand side of the governing equations are transformed into boundary integral equations as in [25]

$$c_i \psi_i^{(s+1)} + \int_\Gamma \left( q_\psi^* \psi^{(s+1)} - u_\psi^* \frac{\partial \psi^{(s+1)}}{\partial n} \right) d\Gamma = \int_\Omega b_1 u_\psi^* d\Omega, \tag{23}$$

$$c_i w_i^{(s+1)} + \int_\Gamma \left( q_w^* w^{(s+1)} - u_w^* \frac{\partial w^{(s+1)}}{\partial n} \right) d\Gamma = \int_\Omega b_2 u_w^* d\Omega, \tag{24}$$

$$c_i T_i^{(s+1)} + \int_\Gamma \left( q_T^* T^{(s+1)} - u_T^* \frac{\partial T^{(s+1)}}{\partial n} \right) d\Gamma = \int_\Omega b_3 u_T^* d\Omega, \tag{25}$$

where  $c_i$  are the constants which depend on whether the source point  $i$  lies in the interior ( $c_i = 1, i = 1, \dots, K_I$ ) or on the smooth boundary ( $c_i = \frac{1}{2}, i = 1, \dots, K_B$ ).

The domain integrals caused by the inhomogeneous terms are transformed to the boundary integral equations using the DRBEM idea as in [22],[25]. To this aim the inhomogeneous terms are expanded as

$$b_1 = \sum_{j=1}^{K_B+K_I} \alpha_{1j} f_j(x, y), \tag{26}$$

$$b_2 = \sum_{j=1}^{K_B+K_I} \alpha_{2j}(t) \bar{f}_j(x, y), \tag{27}$$

$$b_3 = \sum_{j=1}^{K_B+K_I} \alpha_{3j}(t) \bar{f}_j(x, y). \tag{28}$$

Here  $K_B$  and  $K_I$  are the number of the boundary and interior points, respectively.  $\alpha_{1j}, \alpha_{2j}(t)$  and  $\alpha_{3j}(t)$  are initially unknown coefficients.  $f_j = 1+r$  and  $\bar{f}_j = r^2 \log r$  are the coordinate functions.  $f_j$  and  $\bar{f}_j$  are related to particular solutions  $\widehat{\psi}_j$ , and  $\widehat{w}_j, \widehat{T}_j$  as

$$\nabla^2 \widehat{\psi}_j = f_j, \tag{29}$$

$$\nabla^2 \widehat{w}_j - \lambda_w^2 \widehat{w}_j = \overline{f}_j, \quad (30)$$

$$\nabla^2 \widehat{T}_j - \lambda_T^2 \widehat{T}_j = \overline{f}_j. \quad (31)$$

After inserting  $f_j$  and  $\overline{f}_j$  into the corresponding inhomogeneous terms in Equations (26)-(28), we have the Laplace and modified Helmholtz operators inside the domain integrals

$$c_i \psi_i^{(s+1)} + \int_{\Gamma} \left( q_{\psi}^* \psi^{(s+1)} - u_{\psi}^* \frac{\partial \psi^{(s+1)}}{\partial n} \right) d\Gamma = \sum_{j=1}^{K_B+K_I} \alpha_{1j} \int_{\Omega} (\nabla^2 \widehat{\psi}_j) u_{\psi}^* d\Omega, \quad (32)$$

$$c_i w_i^{(s+1)} + \int_{\Gamma} \left( q_w^* w^{(s+1)} - u_w^* \frac{\partial w^{(s+1)}}{\partial n} \right) d\Gamma = \sum_{j=1}^{K_B+K_I} \alpha_{2j}(t) \int_{\Omega} (\nabla^2 \widehat{w}_j - \lambda_w^2 \widehat{w}_j) u_w^* d\Omega, \quad (33)$$

$$c_i T_i^{(s+1)} + \int_{\Gamma} \left( q_T^* T^{(s+1)} - u_T^* \frac{\partial T^{(s+1)}}{\partial n} \right) d\Gamma = \sum_{j=1}^{K_B+K_I} \alpha_{3j}(t) \int_{\Omega} (\nabla^2 \widehat{T}_j - \lambda_T^2 \widehat{T}_j) u_T^* d\Omega. \quad (34)$$

Now the DRBEM idea can be used for the domain integrals appearing on the right hand sides of Equations (32)-(34) in order to obtain the boundary integrals.

$$\begin{aligned} c_i \psi_i^{(s+1)} &+ \int_{\Gamma} \left( q_{\psi}^* \psi^{(s+1)} - u_{\psi}^* \frac{\partial \psi^{(s+1)}}{\partial n} \right) d\Gamma \\ &= \sum_{j=1}^{K_B+K_I} \alpha_{1j} \left[ c_i \widehat{u}_{\psi ij} + \int_{\Gamma} \left( q_{\psi}^* \widehat{u}_{\psi j} - u_{\psi}^* \frac{\partial \widehat{u}_{\psi j}}{\partial n} \right) d\Gamma \right], \end{aligned} \quad (35)$$

$$\begin{aligned} c_i w_i^{(s+1)} &+ \int_{\Gamma} \left( q_w^* w^{(s+1)} - u_w^* \frac{\partial w^{(s+1)}}{\partial n} \right) d\Gamma \\ &= \sum_{j=1}^{K_B+K_I} \alpha_{2j}(t) \left[ c_i \widehat{u}_{w ij} + \int_{\Gamma} \left( q_w^* \widehat{u}_{w j} - u_w^* \frac{\partial \widehat{u}_{w j}}{\partial n} \right) d\Gamma \right], \end{aligned} \quad (36)$$

$$\begin{aligned} c_i T_i^{(s+1)} &+ \int_{\Gamma} \left( q_T^* T^{(s+1)} - u_T^* \frac{\partial T^{(s+1)}}{\partial n} \right) d\Gamma \\ &= \sum_{j=1}^{K_B+K_I} \alpha_{3j}(t) \left[ c_i \widehat{u}_{T ij} + \int_{\Gamma} \left( q_T^* \widehat{u}_{T j} - u_T^* \frac{\partial \widehat{u}_{T j}}{\partial n} \right) d\Gamma \right]. \end{aligned} \quad (37)$$

After discretizing the boundary using  $K_B$  constant elements and taking  $K_I$  interior nodes, the ultimate form of Equation (35)-(37) can be written as one global scheme in a matrix form for both boundary and interior nodes as

$$\begin{aligned}
 H\psi - Gq_\psi &= (H\widehat{\psi} - G\widehat{Q}_\psi)\alpha_1, \\
 H'w + G'q_w &= (H'\widehat{W} + G'\widehat{Q}_w)\alpha_2, \\
 H'T + G'q_T &= (H'\widehat{T} + G'\widehat{Q}_T)\alpha_3,
 \end{aligned}
 \tag{38}$$

where  $\widehat{\psi}, \frac{\partial \widehat{\psi}}{\partial n} = \widehat{Q}_\psi, \widehat{W}, \frac{\partial \widehat{W}}{\partial n} = \widehat{Q}_w, \widehat{T}, \frac{\partial \widehat{T}}{\partial n} = \widehat{Q}_T$  are matrices formed columnwise from the corresponding particular solutions and their normal derivatives. By using the relations in Equation (29)-(31), the particular solutions are obtained as

$$\widehat{\psi} = \frac{r^2}{4} + \frac{r^3}{9}
 \tag{39}$$

and

$$\widehat{Y} = \begin{cases} -\frac{4}{\lambda^4}(K_0(\lambda r) + \log r) - \frac{r^2 \log r}{\lambda^2} - \frac{4}{\lambda^4}, & r > 0 \\ \frac{4}{\lambda^4}(\gamma + \log(\frac{\lambda}{2})) - \frac{4}{\lambda^4}, & r = 0, \end{cases}
 \tag{40}$$

where  $\widehat{Y}$  represents  $\widehat{W}$  and  $\widehat{T}$ ,  $\lambda$  represents  $\lambda_w$  and  $\lambda_T$ . Here the definition of  $r$  is  $r^2 = r_x^2 + r_y^2$  where  $r_x$  and  $r_y$  are the components of  $r$  in the direction of  $x$  and  $y$  axes.

The entries of the matrices  $H, G, H'$  and  $G'$  are defined on the boundary elements  $\Gamma_j$  as in [22, 26, 27]

$$\begin{aligned}
 H_{i,j} &= ci\delta_{ij} + \frac{1}{2\pi} \int_{\Gamma_j} \frac{\partial}{\partial n} \left( \ln \left( \frac{1}{r_i} \right) \right) d\Gamma_j, \\
 G_{i,j} &= \frac{1}{2\pi} \int_{\Gamma_j} \ln \left( \frac{1}{r_i} \right) d\Gamma_j, \\
 H'_{i,j} &= ci\delta_{ij} + \frac{1}{2\pi} \int_{\Gamma_j} \frac{\partial}{\partial n} (K_0(\lambda r_i)) d\Gamma_j, \\
 G'_{i,j} &= \frac{1}{2\pi} \int_{\Gamma_j} K_0(\lambda r_i) d\Gamma_j
 \end{aligned}
 \tag{41}$$

where  $\delta_{ij}$  Kronecker delta function,  $\Gamma_j$  is the  $j$ -th boundary element and  $\lambda$  refers to  $\lambda_w$  and  $\lambda_T$ .

The collocation of the inhomogeneities at  $K_B + K_I$  points results in the systems for  $\alpha_k, (k = 1, 2, 3)$

$$\begin{aligned}
\mathbf{b}_1 &= \mathbf{F}\boldsymbol{\alpha}_1 \Rightarrow \boldsymbol{\alpha}_1 = \mathbf{F}^{-1}\mathbf{b}_1, \\
\mathbf{b}_2 &= \bar{\mathbf{F}}\boldsymbol{\alpha}_2 \Rightarrow \boldsymbol{\alpha}_2 = \bar{\mathbf{F}}^{-1}\mathbf{b}_2, \\
\mathbf{b}_3 &= \bar{\mathbf{F}}\boldsymbol{\alpha}_3 \Rightarrow \boldsymbol{\alpha}_3 = \bar{\mathbf{F}}^{-1}\mathbf{b}_3,
\end{aligned} \tag{42}$$

where  $\mathbf{F}$  and  $\bar{\mathbf{F}}$  are the coordinate matrices constructed by taking  $f_j = 1 + r_j$  and  $\bar{f}_j = r_j^2 \ln r_j$  as columns.

Substituting the  $\boldsymbol{\alpha}_1, \boldsymbol{\alpha}_2, \boldsymbol{\alpha}_3$  into equation (38), the final system of equations for the unknown vectors  $\psi, w$ , and  $T$  can be given as

$$\begin{aligned}
H\psi^{(s+1)} - Gq_\psi^{(s+1)} &= (H\widehat{\psi} - G\widehat{Q}_\psi)F^{-1}b_1^{(s)}, \\
H'w^{(s+1)} + G'q_w^{(s+1)} &= (H'\widehat{W} + G'\widehat{Q}_w)\bar{F}^{-1}b_2^{(s)}, \\
H'T^{(s+1)} + G'q_T^{(s+1)} &= (H'\widehat{T} + G'\widehat{Q}_T)\bar{F}^{-1}b_3^{(s)}.
\end{aligned} \tag{43}$$

In this system all the square matrices have the size  $(K_B + K_I) \times (K_B + K_I)$  and all the vectors have size  $(K_B + K_I) \times 1$ .

First and second derivatives of the variables located in  $\mathbf{b}_i$ , ( $i = 1, 2, 3$ ) can be approximated as

$$\frac{\partial \mathbf{S}}{\partial x} = \frac{\partial \bar{\mathbf{F}}}{\partial x} \bar{\mathbf{F}}^{-1} \mathbf{S}, \quad \frac{\partial \mathbf{S}}{\partial y} = \frac{\partial \bar{\mathbf{F}}}{\partial y} \bar{\mathbf{F}}^{-1} \mathbf{S}, \tag{44}$$

where  $\mathbf{S}$  represents  $\mathbf{w}^{(s)}$ ,  $\psi^{(s+1)}$  and  $\mathbf{T}^{(s)}$ . Also, we need  $\nabla^2 \mathbf{w}^{(s)}$  and  $\nabla^2 \mathbf{T}^{(s)}$ , and they can be obtained by using the coordinate matrix  $\bar{\mathbf{F}}$  such that

$$\nabla^2 \mathbf{S} = \frac{\partial \bar{\mathbf{F}}}{\partial x} \bar{\mathbf{F}}^{-1} \left( \frac{\partial \mathbf{S}}{\partial x} \right) + \frac{\partial \bar{\mathbf{F}}}{\partial y} \bar{\mathbf{F}}^{-1} \left( \frac{\partial \mathbf{S}}{\partial y} \right). \tag{45}$$

The boundary conditions for vorticity are determined by taking the curl of the velocity vector and with the help of the DRBEM coordinate matrix  $\bar{\mathbf{F}}$  as

$$w = \frac{\partial v}{\partial x} - \frac{\partial u}{\partial y} \Rightarrow w = \frac{\partial \bar{\mathbf{F}}}{\partial x} \bar{\mathbf{F}}^{-1} \mathbf{v} - \frac{\partial \bar{\mathbf{F}}}{\partial y} \bar{\mathbf{F}}^{-1} \mathbf{u}. \tag{46}$$

A system of linear equations for the variables  $(\psi-w-T)$  can be constructed by using the equations (43) and by inserting the corresponding known boundary conditions as

$$\begin{aligned}
\mathbf{A}_1 \mathbf{x}_1 &= \mathbf{y}_1, \\
\mathbf{A}_2 \mathbf{x}_2 &= \mathbf{y}_2, \\
\mathbf{A}_3 \mathbf{x}_3 &= \mathbf{y}_3.
\end{aligned} \tag{47}$$

Here,  $\mathbf{x}_1, \mathbf{x}_2$  and  $\mathbf{x}_3$  are constructed by using the unknown information of variables and their normal derivatives. These system of linear equations are obtained for both direct and inverse problems. Any numerical method can be used to obtain

the unknown  $\mathbf{x}_i$ , ( $i = 1, 2, 3$ ) in the solution of the direct problem. Thus, some part of the known temperature boundary conditions are prepared in order to use as a sensor in the solution of the inverse problem. In the solution procedure of the inverse problem, similar to the solution of direct problem, the classical DRBEM can be used to obtain  $\mathbf{x}_1$  and  $\mathbf{x}_2$ . However, the system  $\mathbf{A}_3 \mathbf{x}_3 = \mathbf{y}_3$  for the inverse temperature equation is ill-conditioned and it needs to use any regularization method to obtain a regularized solution. In this study, Tikhonov regularization method [23] is preferred since it is simple compared to the other regularization methods [16]. In the regularization procedure, the system  $\mathbf{A}_3 \mathbf{x}_3 = \mathbf{y}_3$  is written in the form

$$(\mathbf{A}_3^T \mathbf{A}_3 + \lambda \mathbf{I}) \mathbf{x}_3 = \mathbf{A}_3^T \mathbf{y}_3. \quad (48)$$

Here to obtain stable regularized solutions positive regularization parameter  $\lambda$  should be chosen carefully.

In the measurement of the temperature  $T_m$  at the right wall small random errors inherently occur and these errors cause big instability in the solution of the inverse problem. These measurement errors are taken into account by adding random noise data to the temperature  $T(0, y, t) = T_m$  obtained at the right wall from the direct problem as

$$T_m^{noise}(0, y, t) = T_m(0, y, t)(1 + \epsilon\rho), \quad y \in (0, 1), \quad (49)$$

where  $\rho$  is the percentage of the noise and  $\epsilon$  is a random variable in the interval  $[-1, 1]$  generated by IMSL library subroutines RNUN and SSCAL.

## 5. NUMERICAL RESULTS

In this study, DRBEM application is derived for the unsteady natural convection problem in a square cavity filled with  $Cu$ -water based nanofluid with three different Neumann type boundary conditions, which are imposed at the right wall and are steady heat flux ( $q(y) = -\cos(\pi y)$ ), time dependent uniform heat flux ( $q(t) = -\sin(\pi t/t_f)$ ) and non-uniform time dependent heat flux ( $q(y, t) = -\sin(\pi t) \cos(\pi y)$ ), depicted in Figure (1). The numerical results are discussed by using graphs to emphasize the effect of  $Ra$ ,  $\lambda$ ,  $\rho$ , and  $\phi$  on the fluid behaviour. For the computation of both direct and inverse problem, the stopping criteria is taken as  $10^{-5}$ . In order to achieve steady-state results by using a small number of iterations, the relaxation parameters are taken  $\theta_w = \theta_T = 0.9$  [27].

At the beginning of the procedure, the forward finite difference approximation is used for both the time derivatives in the vorticity transport and in the temperature equations. Since forward finite difference scheme is an explicit method, the choice of  $\Delta t$  is an important point for the stability of the solutions. Also, in the modified Helmholtz equations,  $\Delta t$  is located in the parameters  $\lambda_w$  and  $\lambda_T$ . So there is a close relation between the behavior of function  $K_0(x)$  and the choice of  $\Delta t$ . Since  $K_0(x)$  goes to infinity as  $x$  goes to infinity, too small  $\Delta t$  can lead to unstable solutions. In this present study,  $\Delta t$  values used in the computations changes between 0.01 to 0.1.

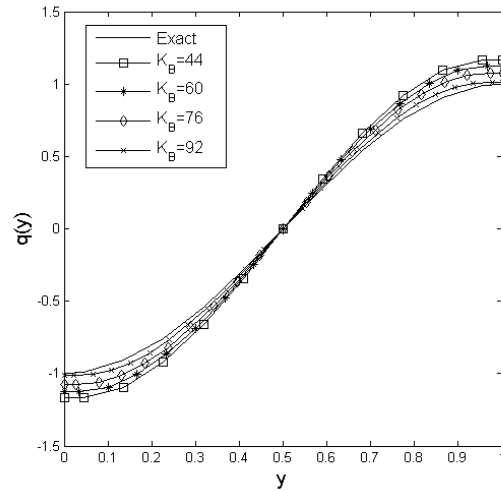


FIGURE 2. Grid Independence of the study for  $\lambda = 10^{-6}$ ,  $Ra = 10^2$ ,  $\phi = 0.05$  and  $\rho = 0$  for Case I.

5.1. **Case I: Steady heat flux.** In this case, heat flux is considered as

$$q(y) = -\cos(\pi y) \quad (50)$$

which depends only on the coordinates of space variable  $y$ . Grid independence test has been done for the steady heat flux case and results are presented for the values  $Ra = 10^2$ ,  $\phi = 0.05$ ,  $\lambda = 10^{-6}$  and  $\rho = 0$  in Figure (2). As can be seen from the figure,  $K_B = 92$  constant boundary elements provides grid independence. Therefore,  $K_B = 92$  is used in all analysis of the rest of the study.

In Figure (3) the effect of the regulation parameter  $\lambda$  is presented within the range  $\lambda = 10^{-4}$  to  $\lambda = 10^{-7}$ . From this figure it can be seen that when the regularization parameter  $\lambda$  takes the higher values than  $10^{-5}$  and takes the smaller values than  $10^{-7}$ , the numerical results becomes unstable which is expected behavior for the ill-posed system.

The effect of Rayleigh number on the steady heat flux is presented in Figure (4). From the figure it can be observed that the behavior of the inverse solution for heat flux are similar to each other for all values of Rayleigh number. The best result is obtained when  $Ra = 10^3$ . As the Rayleigh number decreases up to  $Ra = 0$ , the difference between the exact and inverse solutions starts to grow especially near the top and bottom right corners of the domain. When  $Ra = 10^4$  an improvement occurs in the results. But when the Rayleigh number takes the higher values, for instance  $Ra = 10^5$ , the inverse solutions lose the accuracy and stability.  $Ra = 0$

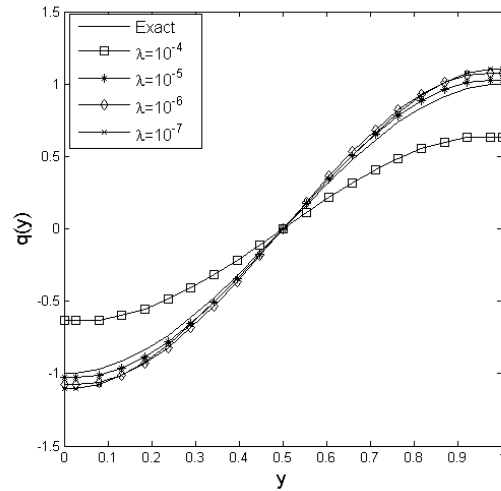


FIGURE 3. Variation of heat flux  $q(y)$  for several values of  $\lambda$  when  $Ra = 10^2$ ,  $\phi = 0.05$  and  $\rho = 0$  for Case I.

means that the system is pure conduction, and the heat transfer mechanism is dominated by conduction up to  $Ra = 10^3$ . For  $Ra = 10^4$ , the heat transfer occurs in the system by convection. So, the worsening behavior of the inverse solution can be explained by the change in behavior in the system caused by the increase in Rayleigh number.

The heat flux obtained from the inverse problem for each iteration up to  $t = 0.5$  is drawn as a global heat flux in Figure (5). For lower values of Rayleigh number (up to  $Ra = 10^2$ ), the results closely follow the global heat flux obtained by the exact solution given by Equation (50). On the other hand, at the beginning of the iterative solution procedure for the higher values of Rayleigh number (up to  $Ra = 10^4$ ), a deflection is observed. Then, when the time achieves  $t = 0.2$ , this deflection disappears, and both exact and inverse solutions become compatible with each other.

For the same analysis, the isotherms are given for  $t = 0.5$  in Figure (6). As can be noticed from the figure, since the heat transfer mechanism is dominated by the conduction up to  $Ra = 10^3$ , there is no considerable change over the isotherms. This means that the convection in the system is weak and it can not be effective on the heat transfer in the system. Also, for all values of Rayleigh number, the isotherms obtained both direct and inverse problem are well matched with the each other.

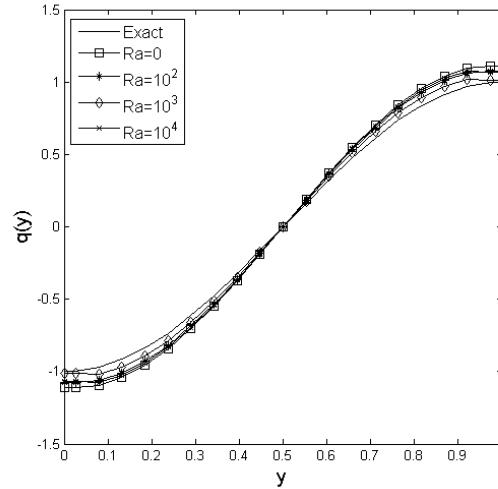


FIGURE 4. Variation of heat flux  $q(y)$  for several values of  $Ra$  when  $\lambda = 10^{-6}$ ,  $\phi = 0.05$  and  $\rho = 0$  for Case I.

The variation in heat flux at different solid volume fraction ( $0 \leq \phi \leq 0.05$ ) is displayed in Figure (7). There is no significant effect of solid volume fraction on heat flux when  $Ra = 0$  and  $Ra = 10^2$ . On the other hand, from the figure it can be concluded that when Rayleigh number takes the values  $Ra = 10^3$  and  $Ra = 10^4$ , the accuracy of the inverse solution improves as the solid volume fraction increases from 0 to 0.05.

**5.2. Case II: Time dependent uniform heat flux.** As a second case, heat flux is considered as

$$q(t) = -\sin(\pi t/t_f), \quad (51)$$

where all the computations are performed for the total simulation time  $t_f = 1$ . In order to compare the effects of steady and time dependent heat fluxes, the same analyses are done as in the previous case. For both direct and inverse problems, the time dependent heat flux, the time dependent global heat flux and the isotherms are drawn in Figures (8)-(10) for the Rayleigh numbers  $0 \leq Ra \leq 10^4$ , respectively. First, the influence of Rayleigh number on the accuracy of the time dependent heat flux obtained from the inverse problem is investigated and is illustrated in Figure (8). From this figure, when the Rayleigh number takes the values between 0 to  $10^3$ , the heat fluxes obtained from the inverse problems are very close to each other. Besides, similar to the steady heat flux case, there is an improvement in the graph for the value of  $Ra = 10^4$ . For the convection dominated system, it cannot be possible to get an accurate results for the heat flux.

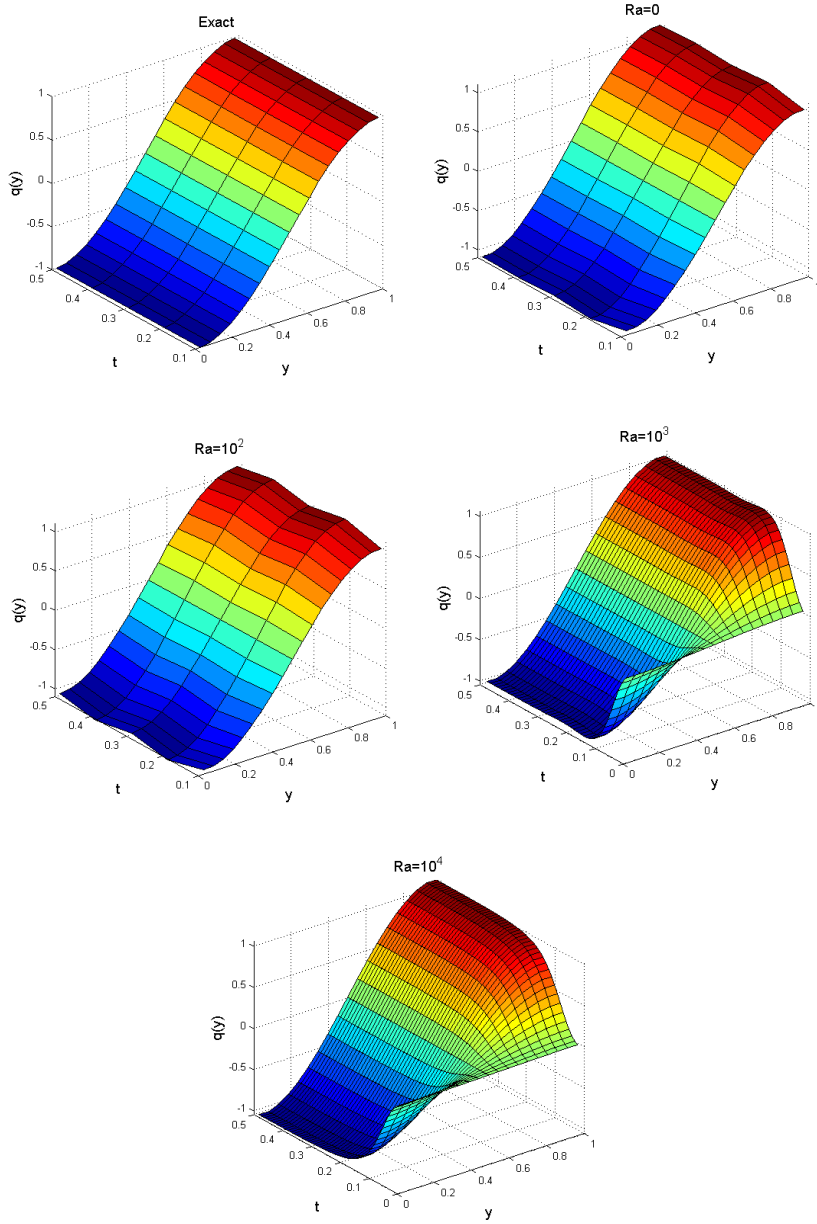


FIGURE 5. Variation of global heat flux for several values of  $Ra$  when  $\lambda = 10^{-6}$ ,  $\phi = 0.05$  and  $\rho = 0$  for Case I.

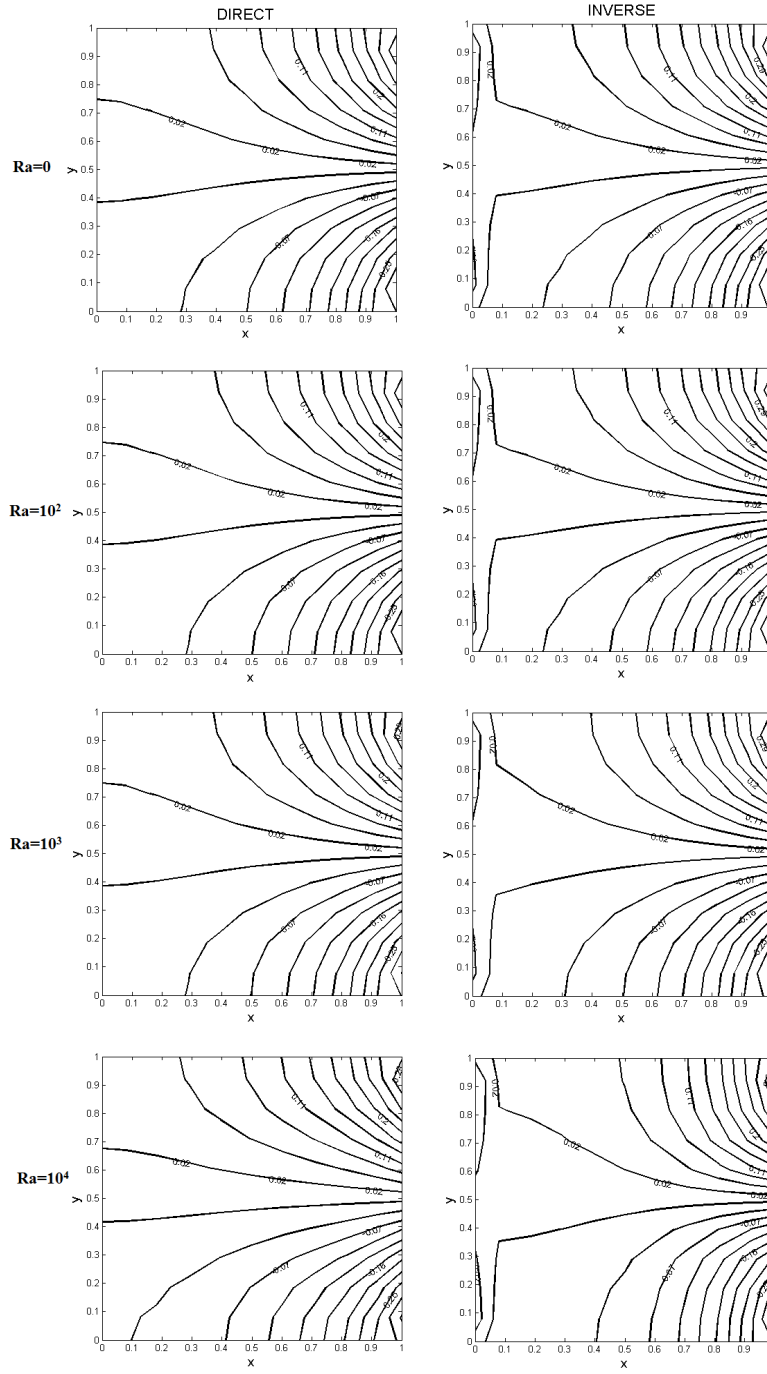


FIGURE 6. Variation of temperature for several values of  $Ra$  when  $\lambda = 10^{-6}$ ,  $\phi = 0.05$  and  $\rho = 0$  for Case I.

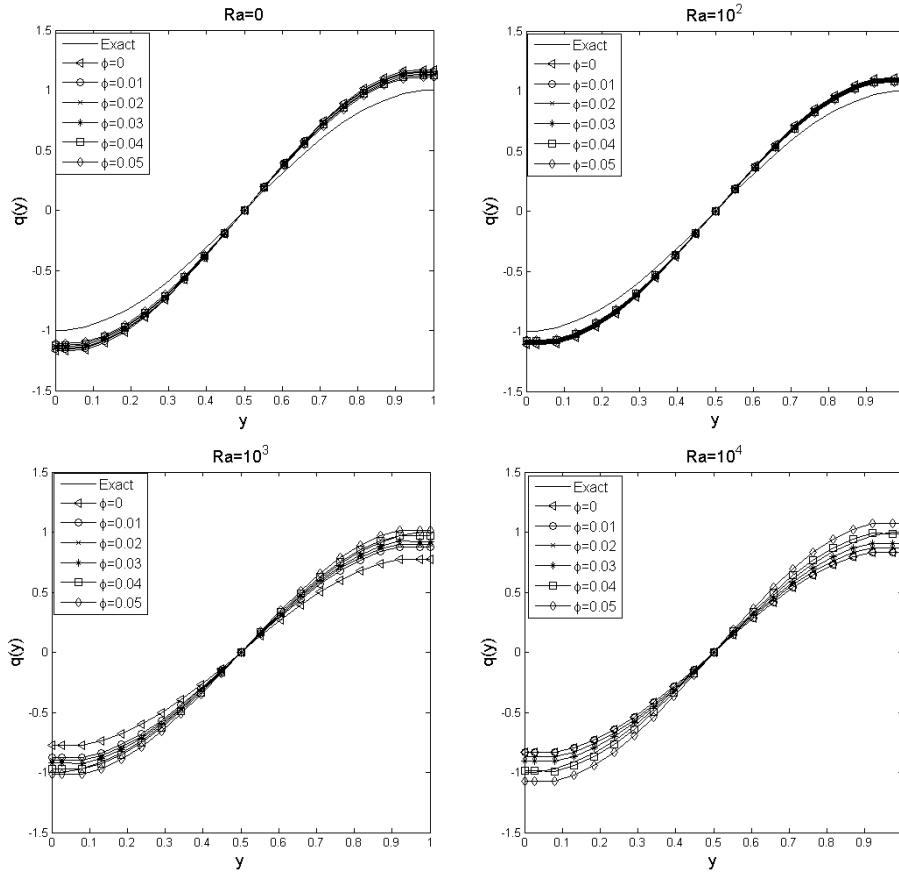


FIGURE 7. Variation of heat flux  $q(y,t)$  for several values of  $\phi$  when  $\lambda = 10^{-6}$  and  $\rho = 0$  for Case I.

The global heat flux for the unsteady case is presented in Figure (9) which is depicted for each iteration up to  $t = 1.0$ . By comparing Figures (5) and (9), it can be seen that in the unsteady case the global heat flux obtained from the direct and inverse problems are in good agreement with each other for all values of Rayleigh number.

Figure (10) shows the effect of the variation of Rayleigh numbers on the isotherms at  $t = 0.5$ . From the figure, the effect of convective forces on heat transfer mechanism can be seen clearly. When the system is dominated by conduction, the isotherms are parallel to the vertical walls. But as the Rayleigh number increases,

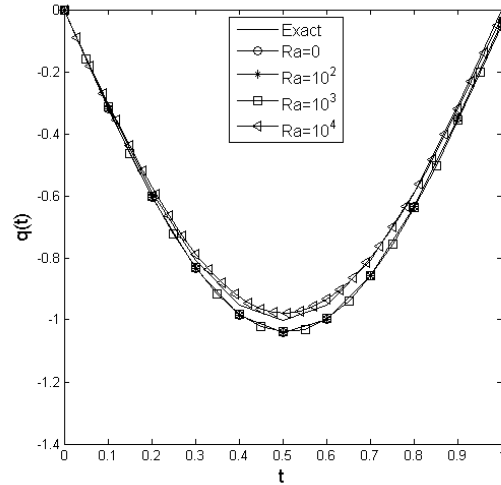


FIGURE 8. Variation of heat flux  $q(t)$  at  $y = 0.5$  for several values of  $Ra$  when  $\lambda = 10^{-6}$ ,  $\phi = 0.05$  and  $\rho = 0$  for Case II.

the isotherms are curled near the top right and the bottom left corners of the domain. These behaviors of isotherm can be observed from the solutions of both the direct and inverse problems.

Figures (11) shows the effect of volume fraction for different Rayleigh numbers on the unsteady heat flux. Similar to the steady case, as Rayleigh number increases from 0 to  $10^2$ , there is no remarkable effect of changes of volume fraction on the heat flux. However after the Rayleigh number reaches  $10^3$  and  $10^4$ , as the volume fraction increases from 0 to 0.05, the inverse solutions approach to the exact values.

**5.3. Case III: Nonuniform time dependent heat flux.** As the last case, heat flux is considered as

$$q(y, t) = -\sin(\pi t) \cos(\pi y) \quad (52)$$

which is nonuniform time-dependent boundary condition. The Rayleigh number effect is reported by giving the global heat flux simulation and isotherm variation for both direct and inverse problems. In Figure (12) global heat flux is presented for Case III by drawing the heat flux at each iteration up to  $t = 1.0$ . From the figure it can be expressed that the level of agreement between the exact and inverse solutions is better than the solutions in the Case I and Case II.

The corresponding isotherms to the same analysis are presented in Figure (13). From the figures it can be concluded that similar to the steady heat flux case, there is no noticeable difference on the isotherms as the Rayleigh number increases. As in Case I, this situation can be explained by the weak convection in the system.

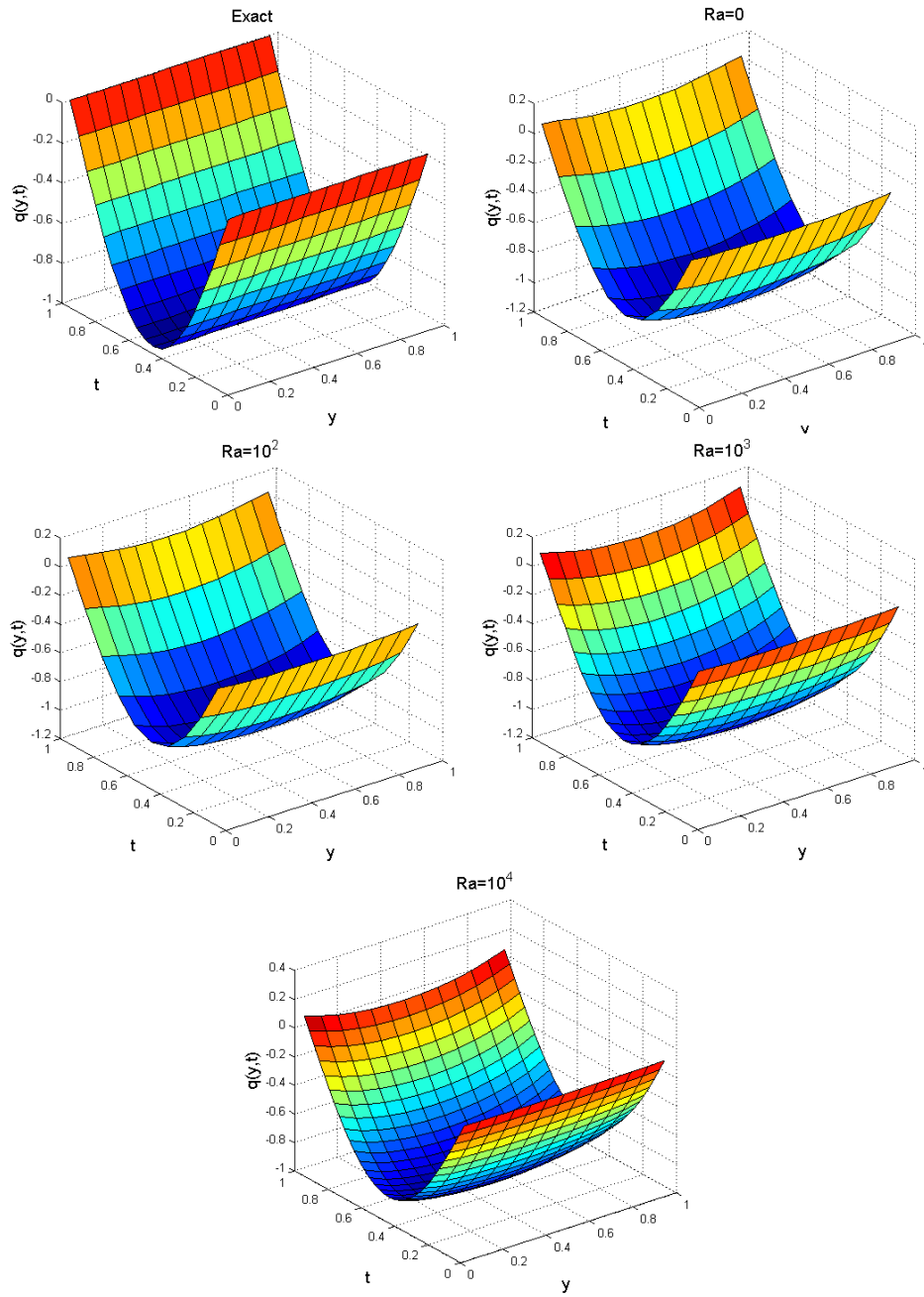


FIGURE 9. Variation of global heat flux for several values of  $Ra$  when  $\lambda = 10^{-6}$ ,  $\phi = 0.05$  and  $\rho = 0$  for Case II.

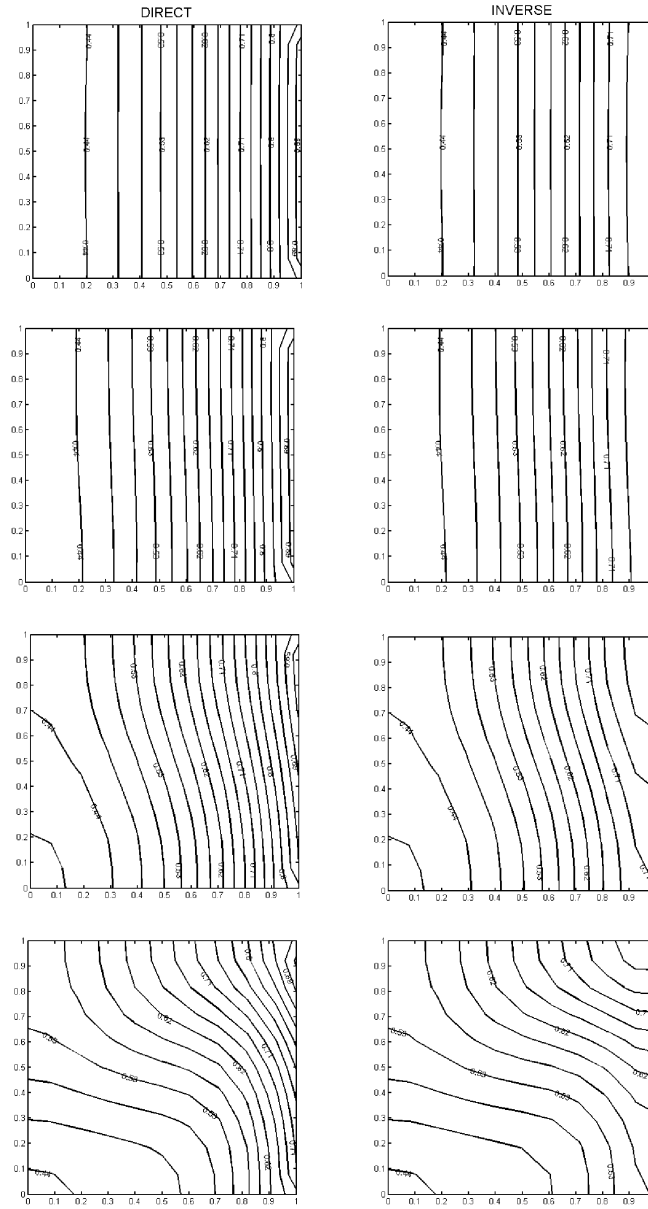


FIGURE 10. Variation of temperature for several values of  $Ra$  when  $\lambda = 10^{-6}$ ,  $\phi = 0.05$  and  $\rho = 0$  for Case II.

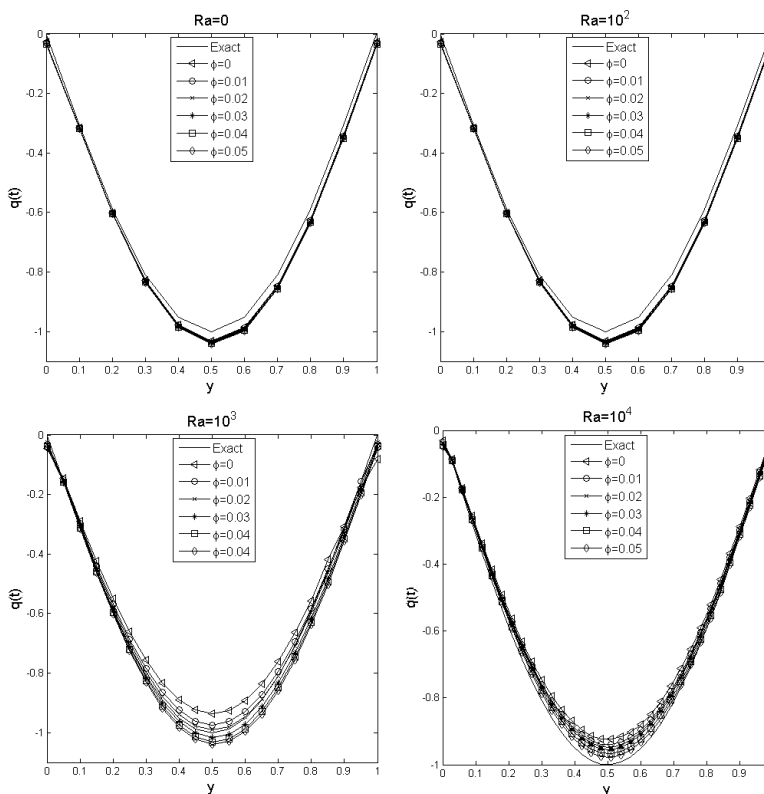


FIGURE 11. Variation of heat flux  $q(t)$  at  $y = 0.5$  for several values of  $\phi$  when  $\lambda = 10^{-6}$  and  $\rho = 0$  for CaseII.

**5.4. The effect of noise.** The last analysis is done to show how the noisy data affects the inverse solutions. For this analysis, the time-dependent heat flux is used which is given in Case II and the numerical results are obtained with the values of the parameters  $Ra = 10^3$ ,  $\phi = 0.05$  and  $\lambda = 10^{-6}$  for several values of percentages of  $\rho \in \{0, 0.01, 0.05\}$ . In the following Figures (14)-(16), the variation in time-dependent heat flux, the global heat flux and the isotherms are shown, respectively.

From the Figure (14) it can be understood that up to  $t = 0.2$ , the noisy data does not affect the heat flux. But after  $t = 0.2$ , there is a deviation occurs for all values of  $\rho$  and this deviation does not grow further and exhibits unchanging behavior up to  $t = 1$ . Particularly for  $\rho = 0.05$ , the deviation in the graphs is much more pronounced than the lower values of  $\rho$ .

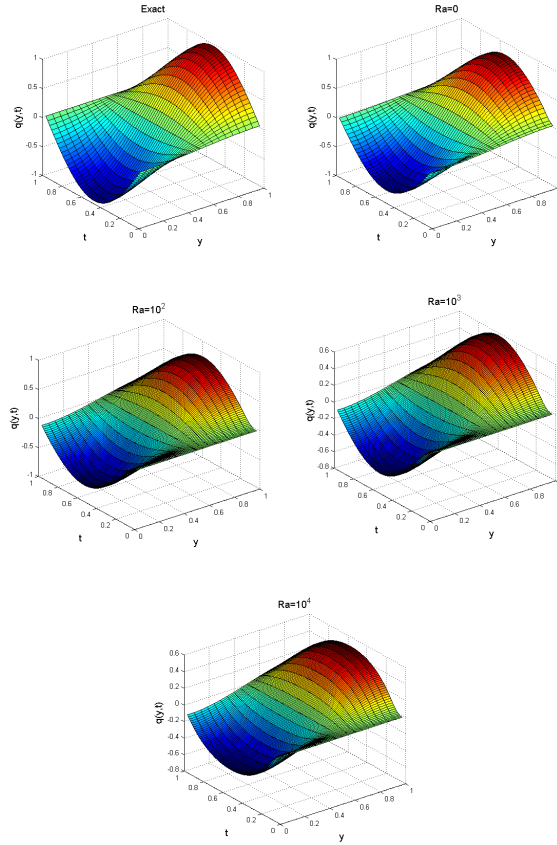


FIGURE 12. Variation of global heat flux for several values of  $Ra$  when  $\lambda = 10^{-6}$ ,  $\phi = 0.05$  and  $\rho = 0$  for Case III.

Similar result can also be inferred from Figure (15). In the case of no noise ( $\rho = 0$ ), the numerical results agree with the exact solution. But when the noisy data is used in the solution of inverse problem, a deflection is occurred in the numerical results, particularly  $\rho = 0.05$ , as  $t$  approaches to the ultimate time 1.

In Figure (16) the isotherms at  $t = 1$  are given to show the effect of noise by comparing with the direct problem solution. From the figures it is clear that the largest deformation occurs at the right wall when the noisy data is used in the solution of inverse problem. In addition, this deformation caused by the noisy data increases with the increased value of the percentage of the  $\rho$ . These expected results

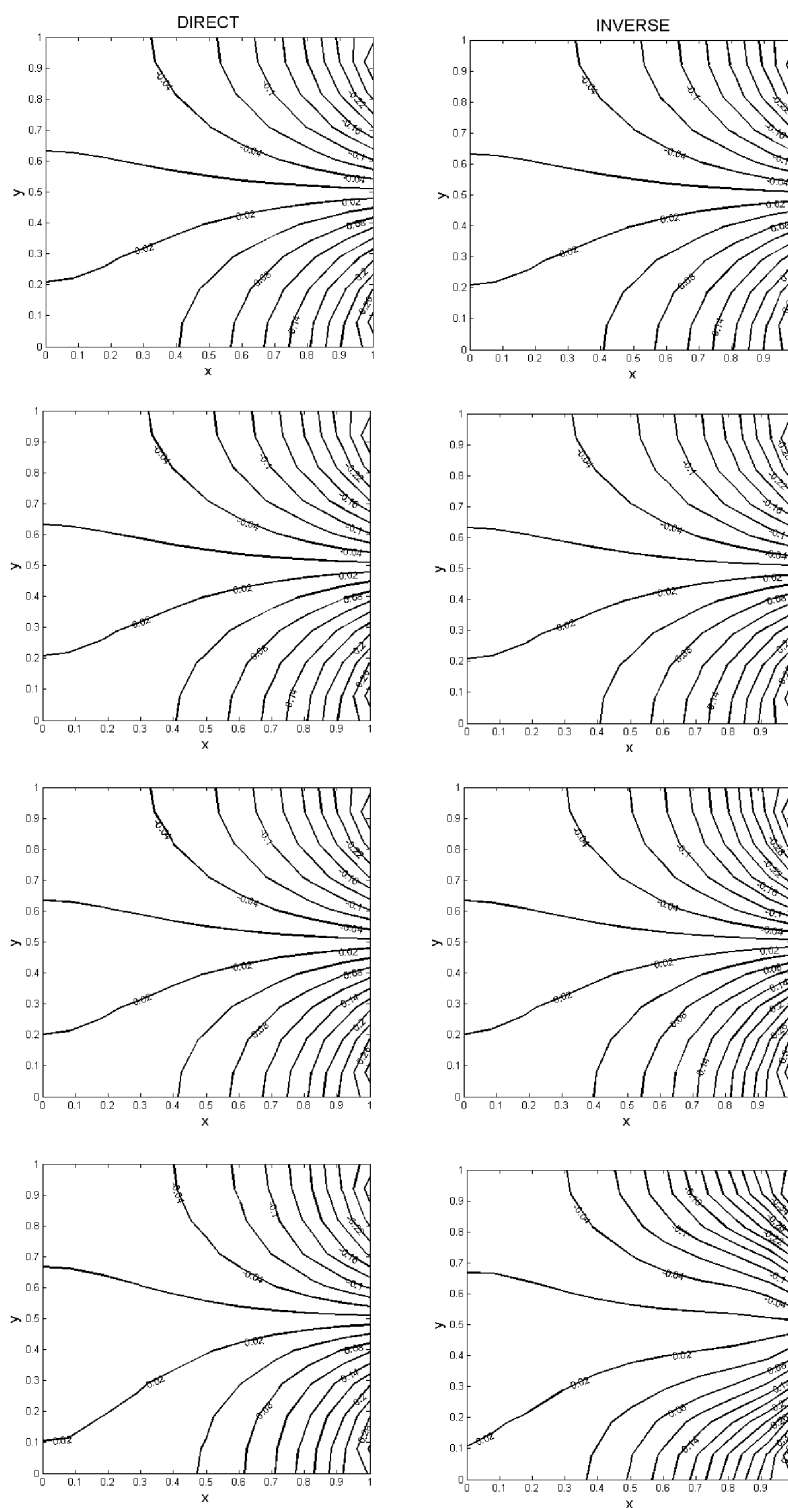


FIGURE 13. Variation of temperature for several values of  $Ra$  when  $\lambda = 10^{-6}$ ,  $\phi = 0.05$  and  $\rho = 0$  for Case III.

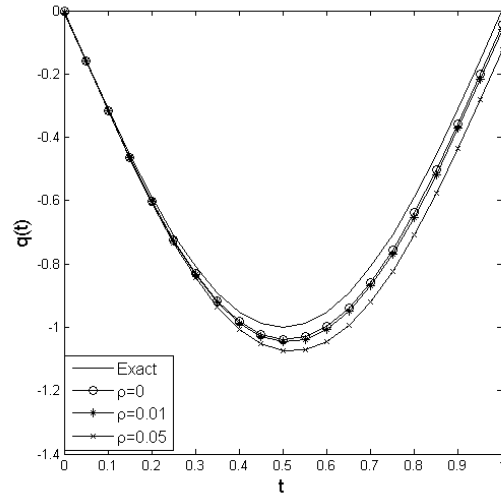


FIGURE 14. Effect of the percentage of the noise  $\rho$  on the heat flux  $q(t)$  at  $y = 0.5$  for  $Ra = 10^3$ ,  $\phi = 0.05$  and  $\lambda = 10^{-6}$  for Case II.

can be explained by the fact that  $T_m$ , which is obtained from the direct problem and considered as a sensor for the inverse problem, is located at the left wall which is the farthest away from right wall. Thus, it can be concluded that the location of the sensor is an important factor for the solution of the inverse problem.

## 6. CONCLUSION

In this study, the solution of two-dimensional unsteady inverse natural convection problem in a square enclosure filled with  $Cu$ -water nanofluid has been obtained by using DRBEM. The method is used for the solutions of both direct and inverse problems. Computations are carried for three types of adiabatic boundary conditions, namely, steady heat flux ( $q(y) = -\cos(\pi y)$ ), time dependent uniform heat flux ( $q(t) = -\sin(\pi t/t_f)$ ) and nonuniform time dependent heat flux ( $q(y, t) = -\sin(\pi t)\cos(\pi y)$ ). DRBEM is an extension of BEM and is used to transform the domain integrals caused by non homogeneous terms of the partial differential equations occurring in the BEM procedure into the boundary integrals. So DRBEM does not need to discretize the domain integrals and this is the main advantage of the method over the domain discretization methods. In the DRBEM

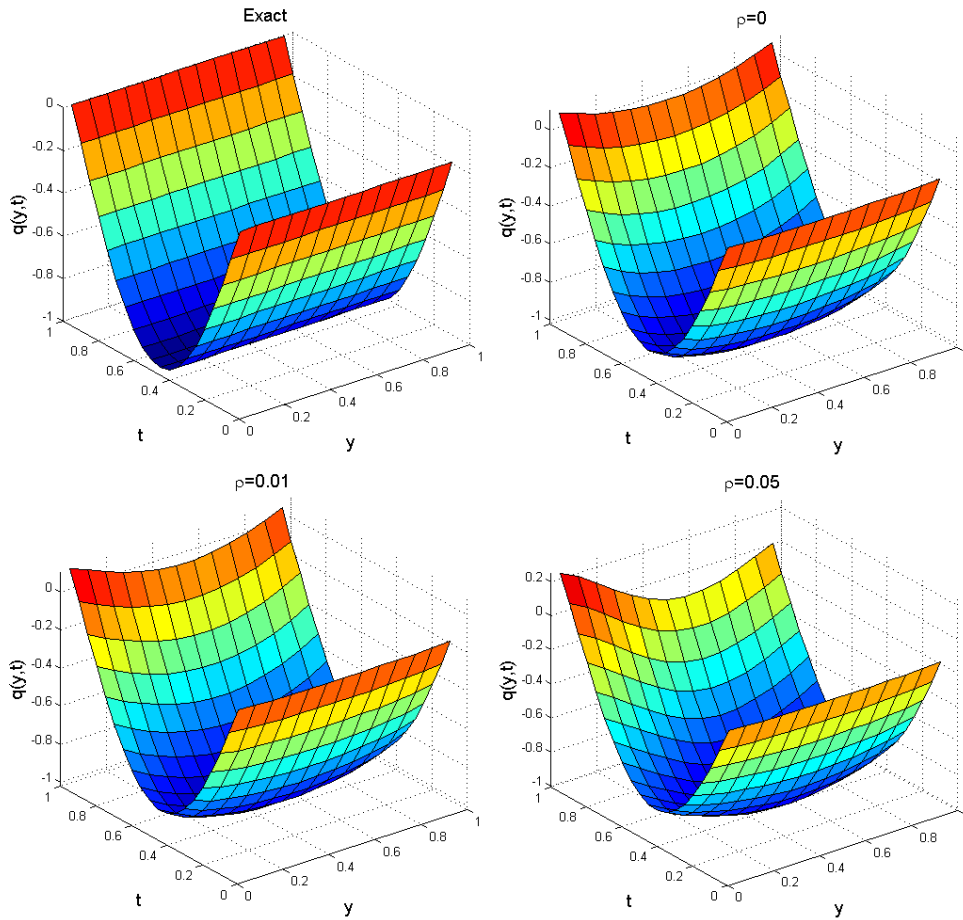


FIGURE 15. Effect of the percentage of the noise  $\rho$  on the global heat flux for  $Ra = 10^3$ ,  $\phi = 0.05$  and  $\lambda = 10^{-6}$  for Case II.

solution procedure, all the terms except the Laplace or modified Helmholtz operators depending on the fundamental solution to be used are considered as nonhomogeneous terms. The nonhomogeneous terms are approximated using the radial basis functions.

The results are given for a range of Rayleigh number ( $0 \leq Ra \leq 10^4$ ), particle volume fraction ( $0 \leq \phi \leq 0.05$ ) and percentage of the noise ( $0 \leq \rho \leq 0.05$ ). The effects of the parameters on the inverse heat flux and isotherm patterns are presented graphically. The results of this study can be summarized as follows:

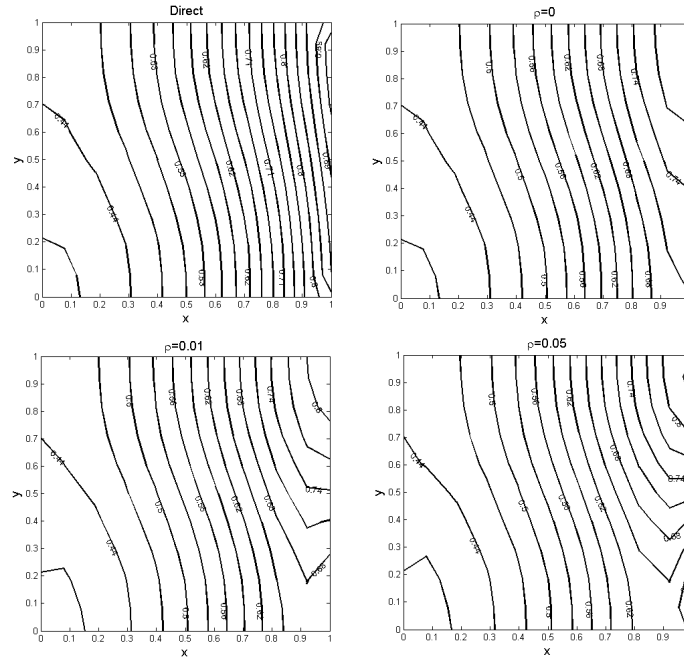


FIGURE 16. Effect of the percentage of the noise  $\rho$  on the Temperature  $T$  for  $Ra = 10^3$ ,  $\phi = 0.05$  and  $\lambda = 10^{-6}$  for Case II.

- The analyses done for different values of Rayleigh number to show that in all three cases the Rayleigh number has a crucial effect in obtaining heat flux from the inverse problem. Reasonable accurate and stable numerical results are obtained at various values of  $Ra$  using both noiseless and noisy temperature data. Especially, it is observed that when the heat transfer mechanism is dominated by weak conduction or convection, the heat flux results obtained from the inverse problem are much better. On the other hand, when the Rayleigh number takes the higher values, it not possible to obtain stable solutions from the inverse problem.
- Accuracy and stability of the inverse solutions also depend on type of the boundary conditions. When the graphics of global heat flux in all three cases are compared, it can be concluded that the closest solutions to the exact solution is obtained by using the non uniform time-dependent heat flux. Also, when steady and non-uniform time-dependent heat fluxes are used, the heat transfer in the system is governed by weak conduction, while it is governed by convection when time-dependent heat flux is used for the same Rayleigh numbers.

- The sensor position becomes key factor to obtain a stable results when the noisy temperature data is used in the solution of inverse problem. As used in this study, if the sensor is located at the left wall which is the farthest away from right wall, the heat flux at the right wall is obtained with larger deformation. In addition, the percentage of the noise is another important factor for the inverse solutions. When the increased value of percentage of the noise is used, the deformation becomes more pronounced.

These results mentioned above are good agreement with the results for the inverse natural convection problem and inverse heat conduction problem in [19] and [17], respectively.

The temperature values at the left wall of the cavity obtained from the direct problem are considered as a sensor for the inverse problem. These values are used as overprescribed boundary condition for the solution of inverse problem. In this case, the accuracy of the solutions of the direct problem at the boundary become quite important. DRBEM enables us to get unknowns and their normal derivatives at the boundary without discretizing the whole domain. Thus, the stable and reasonable accurate results can be obtained at a small computational expense. DRBEM is the most appropriate numerical solution technique for the solution of unsteady inverse natural convection of nanofluid problem. It can be concluded that the DRBEM solutions are well regularized for the inverse problem.

**Declaration of Competing Interest** The author has no competing interests to declare.

#### REFERENCES

- [1] Choi, S. U. S., Eastman, J. A., Enhancing thermal conductivity of fluids with nanoparticles, *ASME Fluids Engineering*, 231 (1995), 99–105.
- [2] Kakaç, S., Pramuanjaroenkij, A., Review of convective heat transfer enhancement with nanofluids, *International Journal of Heat and Mass Transfer*, 52 (13-14) (2009), 3187–3196, <https://doi.org/10.1016/j.ijheatmasstransfer.2009.02.006>.
- [3] Saidur, R., Leong, K. Y., Mohammad, H. A., A review on applications and challenges of nanofluids, *Renewable and Sustainable Energy Reviews*, 25(3) (2011), 1646–1668, <https://doi.org/10.1016/j.rser.2010.11.035>.
- [4] Wang, X. Q., Mujumdar, A.S., A review on nanofluids-part I:Theoretical and numerical investigations, *Brazilian Journal of Chemical Engineering*, 25(4) (2008), 613–630, <https://doi.org/10.1590/S0104-66322008000400001>.
- [5] Wang, X. Q., Mujumdar, A. S., A review on nanofluids-part II:Experiments and applications, *Brazilian Journal of Chemical Engineering*, 25(4) (2008), 631–648, <https://doi.org/10.1590/S0104-66322008000400002>.
- [6] Wen, D., Lin, G., Vafaei, S., Zhang, K., Review of nanofluids for heat transfer applications, *Particuology*, 7(2) (2009), 141–150, <https://doi.org/10.1016/j.partic.2009.01.007>.
- [7] Yu W., France D. M., Routbort J. L., Choi S. U. S., Review and comparison of nanofluid thermal conductivity and heat transfer enhancements, *Heat Transfer Engineering*, 29(5) (2008), 432–460, <https://doi.org/10.1080/01457630701850851>.

- [8] Mahian, O., Kolsi, L., Amani, M., Estelle, P., Ahmadi, G., Kleinstreuer, C., Marshall, J. S., Siavashi, M., Taylor, R. A., Niazmand, H., Wongwises, S., Hayat, T., Kolanjiyil, A., Kasaeian, A. and Pop, I., Recent advances in modeling and simulation of nanofluid flows- Part I: Fundamental and theory, *Physics Reports*, 790 (2019), 1–48, <https://doi.org/10.1016/j.physrep.2018.11.004>.
- [9] Mahian, O., Kolsi, L., Amani, M., Estelle, P., Ahmadi, G., Kleinstreuer, C., Marshall, J.S., Siavashi, M., Taylor, R.A., Niazmand, H., Wongwises, S., Hayat, T., Kolanjiyil, A., Kasaeian, A. and Pop, I., Recent advances in modeling and simulation of nanofluid flows- Part II: Applications, *Physics Reports*, 791 (2019), 1–59, <https://doi.org/10.1016/j.physrep.2018.11.004>.
- [10] Beck, J. V., Blackwell, B., St. Clair, C.R., *Inverse Heat Conduction Ill-Posed Problem*, Wiley, New York, 1985.
- [11] Huang, C. H., Ozisik, M. N., Inverse problem of determining unknown wall heat flux in laminar flow through a parallel plate duct, *Numer. Heat Tr. Part A*, 21(1) (1992), 55–70, <https://doi.org/10.1080/10407789208944865>.
- [12] Rap, A., Elliott, L., Ingham, D. B., Lesnic, D., Wen, X., DRBEM for Cauchy convection-diffusion problems with variable coefficients, *Eng. Anal. Bound. Elem.*, 28(11) (2004), 1321–1333, <https://doi.org/10.1016/j.enganabound.2004.06.003>.
- [13] Lesnic, D., Wake, G. C., A mollified method for the solution of the Cauchy problem for the convection-diffusion equation, *Inverse Prob. Sci. Eng.*, 15(4) (2007), 293–302, <https://doi.org/10.1080/17415970600839002>.
- [14] Ranjbar, Z., Elden, L., Numerical analysis of an ill-posed Cauchy problem for convection-diffusion, *Inverse Prob. Sci. Eng.*, 15(3) (2007), 191–211, <https://doi.org/10.1080/17415970600557299>.
- [15] Lesnic, D., The decomposition method for Cauchy advection-diffusion problems, *Comput. Math. Appl.*, 49(4) (2005), 525–537, <https://doi.org/10.1016/j.camwa.2004.10.031>.
- [16] Marin, L., Elliott, L., Heggs, P. J., Ingham, D. B., Lesnic, D., Wen, X., Dual reciprocity boundary element method solution of the Cauchy problem for Helmholtz-type equations with variable coefficients, *J. Sound Vibration*, 297(1-2) (2006), 89–105, <https://doi.org/10.1016/j.jsv.2006.03.045>.
- [17] Zhuo, L., Lesnic, D., Ismailov, M. I., Tekin, I., Meng, S., Determination of the time-dependent reaction coefficient and the heat flux in a nonlinear inverse heat conduction problem, *Int. J. Computer Mathematics*, 96(10) (2019), 2079–2099, <https://doi.org/10.1080/00207160.2018.1556790>.
- [18] Li, Z. R., Prud'homme, M., Nguyen, T. H., A numerical solution for the inverse natural-convection problem, *Numer. Heat Transfer Part B*, 28(3) (1995), 307–321, <https://doi.org/10.1080/10407799508928836>.
- [19] Prud'homme, M., Nguyen, T. H., Whole time-domain approach to the inverse natural convection problem, *Numer. Heat Transfer Part B*, 32(2) (1997), 169–186, <https://doi.org/10.1080/10407789708913886>.
- [20] Alsoy-Akgün, N., Lesnic, D., A Numerical Solution for an Inverse Natural Magneto-Convection Problem, *Numer. Heat Transfer Part B*, 63(2) (2013), 115–138, <https://doi.org/10.1080/10407790.2013.740978>.
- [21] Aydin, C., Tezer-Sezgin, M., DRBEM solution of the Cauchy MHD duct flow with a slipping perturbed boundary, *Eng. Anal. Bound. Elem.*, 93 (2018), 94–104, <https://doi.org/10.1016/j.enganabound.2018.04.007>.
- [22] Partridge, P. W., Brebbia, C. A., Wrobel, L. C., *The Dual Reciprocity Boundary Element Method*, Computational Mechanics Publications, Southampton, 1992.
- [23] Tikhonov, A. N., Arsenin, V. Y., *Solution of Ill-Posed Problems*, Winstonedsons, Washington, 1977.

- [24] Aminossadati, S. M., Ghasemi, B., Natural convection cooling of a localised heat source at the bottom of a nanofluid-filled enclosure, *European Journal of Mechanics B/Fluids*, 28(5) (2009), 630–640, <https://doi.org/10.1016/j.euromechflu.2009.05.006>.
- [25] Brebbia, C. A., *The Boundary Element Method for Engineers*, Pentech Press, London, 1984.
- [26] Tezer-Sezgin, M., Boundary element method solution of MHD flow in a rectangular duct, *Int. J. for Num. Methods in Fluids*, 18(10) (1994), 937–952, <https://doi.org/10.1002/fld.1650181004>.
- [27] Alsoy-Akgün, N., Tezer-Sezgin, M., DRBEM and DQM solution of natural convection flow in cavity under a magnetic field, *Progr in Comput. Fluid Dynamics*, 13(5) (2013), 270–284, <https://doi.org/10.1504/PCFD.2013.055056>.